Carbon 189 (2022) 548–560

Contents lists available at ScienceDirect

Carbon

journal homepage: www.elsevier.com/locate/carbon

On the deactivation of N-doped carbon materials active sites during oxygen reduction reaction

Javier Quílez-Bermejo [a, *], Emilia Morallón [b], Diego Cazorla-Amorós [a]

[a] Departamento de Química Inorgánica and Instituto de Materiales, Universidad de Alicante, Ap. 99, 03080, Alicante, Spain
[b] Departamento de Química Física and Instituto de Materiales, Universidad de Alicante, Ap. 99, 03080, Alicante, Spain

ARTICLE INFO

Article history:
Received 7 September 2021
Received in revised form
23 December 2021
Accepted 25 December 2021
Available online 28 December 2021

Keywords:
Carbon materials
Nitrogen
Electrocatalysts
Oxygen reduction reaction

ABSTRACT

N-doped carbon materials have been considered one of the most promising options for the replacement of platinum-based electrocatalysts towards the oxygen reduction reaction (ORR). This work provides insights into the deactivation routes of N-doped carbon materials. The changes occurring in the active sites of N-doped carbon catalysts have been analyzed in detail through pre- and post-ORR characterization by XPS of selectively N-doped carbon materials. Moreover, computational modelling was used to deepen into the deactivation mechanism of N-doped carbon materials in the ORR. From XPS and computational modelling, it can be concluded that the deactivation of graphitic-type nitrogen species, during the ORR in both acidic and alkaline environments, occurs through oxidation and tautomerization reactions that result in the formation of N–C–O-type groups. In acidic environment, the reaction kinetics is slower due to the high stability of the ORR intermediates. In alkaline electrolyte, the N–C–O-type groups can be easily formed due to the interaction of graphitic-type N species and the OH^- anions from the electrolyte. In this case, the catalytic activity is due to the contribution of both graphitic nitrogen groups and N–C–O species.

1. Introduction

Fuel cells arise as an attractive alternative towards the replacement of current combustion engines for automotive applications because of their clean conversion of chemical energy to electricity [1,2]. However, one of the main limitations of these electrochemical devices is found in the cathode electrode, where the oxygen reduction reaction (ORR) occurs [3–5]. ORR is a limiting reaction of these devices since it shows sluggish kinetics and high overpotential, which makes necessary the use of high loading of expensive catalysts [6,7]. The current commercial catalyst is based on platinum nanoparticles supported on carbon materials; however, the high cost, low abundance in nature, carbon monoxide poisoning and low stability are some of the main limitations of these cathode electrodes [8–10].

One of the most promising alternatives for replacing platinum-based catalysts consists of the use of metal-free carbon-based catalysts [11,12]. Non-doped carbon materials show a homogeneous distribution of the electron density, which makes difficult the chemisorption of the oxygen molecules. In order to increase the kinetics of ORR in catalysts based on carbon materials, the introduction of heteroatoms is necessary to disturb the electron density distribution and enhance the catalytic activity for ORR [13–15]. In this sense, N-doped carbon materials have demonstrated excellent catalytic properties towards the ORR in experimental [14,16], and computational [17–19] studies. However, there is still controversy about the nature of the active sites. Most of the works that try to shed light on the ORR mechanisms for N-doped carbon materials focus on the identification of the active sites, and a general agreement seems to exist: graphitic N (also known as quaternary N) and pyridine species seem to be the most active sites towards the ORR [16,20,21].

Nevertheless, despite the remarkable performance of these materials and the increase in the knowledge about the active sites, there is still a significant limitation to face; N-doped carbon materials show a non-negligible deactivation with time [22]. This is a factor of paramount importance since the stability of the cathode electrodes is of pivotal relevance for the industrial commercialization of fuel cells. The deactivation mechanisms are extensively studied in the scientific literature for metal-containing catalysts [22]; however, to the best of our knowledge, there exists a lack of

* Corresponding author.
E-mail address: javiq@ua.es (J. Quílez-Bermejo).

https://doi.org/10.1016/j.carbon.2021.12.086

knowledge regarding the deactivation mechanism in metal-free N-doped carbon catalysts. The most common explanation for this issue considers the oxidation of the active sites [23]. Previous work tried to handle this challenging target. By computational modelling, Yang et al. [24] studied the oxidation mechanism of heteroatom-doped carbon-based catalysts for the ORR using unsaturated carbon flakes. They did not consider hydrogen-terminated edges in the carbon material, which is the most stable situation in carbon-based materials. Moreover, despite the interesting theoretical results obtained, the lack of support from experimental results and the non-consideration of the crucial role of the electrolyte make necessary further studies. This last factor, i.e. the role of the electrolyte, is of great importance since such a pH-dependent behaviour of carbon-based catalysts in ORR makes difficult the comprehension of the deactivation mechanism [25].

This work aims to provide further insights into the deactivation mechanism by which metal-free N-doped carbon catalysts reduce their effectiveness for ORR in alkaline and acidic electrolytes. For this purpose, a selectively N-doped carbon material that only contains graphitic-type nitrogen species has been used and the changes occurring in this specific nitrogen species during ORR has been studied by XPS. Computational modelling based on Density Functional Theory (DFT) calculations were performed to unravel the deactivation mechanism for N-doped carbon materials in both acidic and alkaline solutions.

2. Experimental

2.1. Electrocatalysts synthesis

Polyaniline (PANI) was chemically synthesized according to our previous work [26]. 0.067 M of aniline was introduced in stoichiometric ratio with ammonium persulfate in 1.5 L solution of 1 M HCl. Then, the solution was kept under continuous stirring (500 rpm) for 3 h at 0 °C. The obtained polymer was filtered, washed with 2 L of water and dried at 80 °C. Then, the resultant polymer was treated with 1 M NH_4OH for 24 h to obtain the dedoped PANI. The obtained PANI was washed again with distilled water and dried at 80 °C for 12 h.

N-doped carbon material, with the majority of graphitic nitrogen groups, was obtained from the double-stage heat treatment of PANI [20]. First, PANI is treated under an oxygen-containing atmosphere (5000 ppm of O_2 in N_2) at 1000 °C for 1 h using a heating rate of 5 °C min^{-1} and, then, cooled down up to room temperature in the same atmosphere. The flow rate was maintained at 100 mL min^{-1}. The second step is based on a second heat treatment at 1200 °C under an inert (N_2) atmosphere for 1 h using a heating rate of 5 °C min^{-1}. The flow rate for this second treatment was fixed at 150 mL min^{-1}. More details about the characterization of these materials and the synthesis can be found in our previous work [20]. In brief, the first treatment at 1000 °C in an atmosphere containing 5000 ppm of O_2 in N_2 was used to generate a well-developed surface area that makes the active sites accessible to the electrolyte. On the other hand, the second heat treatment at 1200 °C under N_2 was performed to tailor the nitrogen functionalities since pyridines are transformed into graphitic nitrogen species at temperatures above 1000 °C [27,28]. The resultant material shows a BET surface area of 1360 m^2 g^{-1} and a N and O content of 1.4 and 2.8 at.%, respectively. This specific synthetic protocol leads to carbon materials with one nitrogen species: graphitic-type functional groups, being the edge-type graphitic nitrogen groups the active sites for ORR.

2.2. Characterization

The surface composition and oxidation states of the elements of the prepared materials were studied using X-ray photoelectron spectroscopy (XPS) in a VG.Microtech Multilab 3000 spectrometer through radiation of Al Kα (1253.6 eV) and pass energy of 50 eV. The deconvolutions of the XPS spectra have been carried out by using least-squares fitting with Gaussian-Lorentzian curves. The C1s peak at 284.6 eV was used as a reference to position the other peaks. The XPS N1s data were obtained from the average of ten cycles and were analyzed considering the full-width at half-maximum (FWHM) of 1.6 ± 0.2 eV [29]. The error in the binding energies of the nitrogen species in the N1s spectra was ±0.2 eV. For this purpose, we have used polyaniline as a reference material (N1s spectra has been included in Fig. S1). Considering the errors of the FWHM and binding energies, the estimation of the measurements uncertainty of the deconvolution of XPS analysis is 5%.

The electrocatalytic behaviour towards ORR was carried out in an Autolab PGSTAT302 (Metrohm, Netherlands) potentiostat. A rotating ring-disk electrode (RRDE, Pine Research Instruments, USA), equipped with a glassy carbon disk (5.61 mm in diameter) and a platinum ring, was used. A graphite rod was employed as the counter electrode, and a reversible hydrogen electrode (RHE) immersed in the working solution via a Luggin capillary was utilized as the reference electrode. The disk electrode was modified with 120 μg of the sample through the drop-casting of a 1 mg mL^{-1} suspension of the material in a 20% isopropanol, 0.02% Nafion ® aqueous solution, thereby obtaining a catalyst loading of 0.5 mg cm^{-2}. The electrocatalytic activity towards ORR was studied by linear sweep voltammetry (LSV) for alkaline and acid media in O_2-saturated 0.1 M KOH and 0.5 M H_2SO_4, respectively, between 0.0 and 1.0 V at different rotation rates, from 400 to 2025 rpm and at a scan rate of 5 mV s^{-1}. Furthermore, the potential of the ring in RRDE was held constant at 1.5 V vs RHE during all measurements. The number of electrons transferred has been calculated by rotating ring-disk electrode experiments according to hydrogen peroxide oxidation in the Pt ring electrode, as follows:

$$n = \frac{4I_d}{I_d + I_r/N}$$

where I_d and I_r represent the current measured at the disk and ring electrodes, respectively, and N is the collection efficiency of the ring, which was experimentally determined to be 0.37. Before all ORR experiments, the platinum ring is electrochemically cleaned through the 50 cycles at 50 mV s^{-1} between 0.0 and 1.65 V vs RHE, to ensure the removal of organic impurities in the surface of the platinum ring electrode.

Cycling tests were also carried out in O_2-saturated 0.1 M KOH and 0.5 M H_2SO_4 solutions by applying 25 cycles between 1.0 and 0.0 V vs RHE at a scan rate of 5 mV s^{-1}. The E_{ONSET} was measured at a current density of −0.1 mA cm^{-2} for all experiments. In order to study the changes in the catalysts depending on the applied potential, chronoamperometric experiments were also performed at different potentials, from 1.0 V to 0.0 V vs RHE and different time of analysis in an O_2-saturated 0.1 M KOH and 0.5 M H_2SO_4 solutions.

To analyze the changes in the surface composition and oxidation states of the sample after ORR analysis, XPS was performed before and after ORR measurements, including cyclic voltammetry and chronoamperometric analysis (as explained above). For those analyses, a non-rotating glassy carbon electrode was used in which the material is drop-casted as done for the RRDE, and the same electrochemical conditions as those used in the rotating electrode were applied (loading, electrolyte, scan rate, etc.). Then, the glassy carbon electrode was washed with distilled water to remove the excess of KOH or H_2SO_4 and dried in an oven for 12 h at 100 °C to ensure the complete removal of humidity in the XPS experiments, which might interfere in the O1s spectra. After this, XPS analysis

was performed according to the experimental procedure mentioned above.

2.3. Computational modelling

Density functional theory (DFT) at the M06-2X/6-31G(d,p) level was employed in this study through Gaussian 09 software [30], using restricted and unrestricted Hamiltonians for closed- and open-shell systems, respectively. Free energies for ORR steps were computed as the energy differences of the optimized geometries, including vibrational corrections. All energies are reported in eV (1 Hartree = 27.2116 eV). Self-consistent reaction field (SCRF) models of solvation were used with a polarized continuum model (PCM) to represent a precise consideration of the effect of the electrolytes. The carbon flakes consist of a quasi-circular carbon graphene layer formed by 80 atoms with zigzag and armchair edge sites. One N atom is introduced into the carbon matrix according to the chemical nature of the nitrogen functional groups that are studied. Moreover, to obtain more accurate results, the modelling was augmented by the introduction of two water molecules that can reflect explicit hydrogen bonds with the ORR intermediates of the carbon flakes [17,31]. For simulating the acidic environment, one hydronium (H_3O^+) cation was introduced instead of one water molecule for simulating a protonic environment [25].

The energy diagrams of ORR have been calculated based on the Norskov model [32]. In brief, the free energy of all ORR steps is defined as follows: $\Delta G = \Delta E' - T \cdot \Delta S + \Delta G_U$, with $\Delta E'$ being the reaction energy, ΔS represents the variation in entropy and ΔG_U involves the changes in free energy related to the applied electrochemical potential. Moreover, T represents the temperature; in this study, 298 K was selected. $\Delta G_U = n \cdot e \cdot U$, with U being the applied electrode potential and n represents the number of electrons that are involved in each reduction step.

3. Results & discussion

3.1. Experimental results

For this study, we have selected a N-doped carbon material that was prepared in a previous work (NMC) [20]. This material essentially contains graphitic-type nitrogen functional groups, which makes it a perfect model material to further analyze the changes of the active sites upon reaction. Prior to the evaluation of the changes in the chemical state of the NMC sample, this catalyst was tested towards the ORR. Fig. 1 shows the linear sweep voltammetry curves in oxygen-saturated 0.5 M H_2SO_4 and 0.1 M KOH solutions in the first and 25th cycle at working conditions. This test was performed to observe changes in the catalytic activity towards the ORR after cycling the material in working conditions. Fig. S2 shows the current recorded in the platinum ring for the obtention of the number of transferred electrons in these experiments. NMC shows high catalytic activity towards the ORR in alkaline electrolyte with an E_{ONSET} of 0.91 V and a half-wave potential of 0.79 V vs RHE. These results are excellent for metal-free carbon-based electrocatalysts, but they are still far from the commercial platinum-based electrodes, with an E_{ONSET} of 0.98 V and a half-wave potential of 0.86 V vs RHE (Fig. S3). After 25 cycles, the performance of the electrocatalyst slightly decreases to an E_{ONSET} of 0.86 V and a half-wave potential of 0.74 V vs RHE. At a potential below 0.5 V vs RHE, changes in the current in the ORR polarization and the number of electrons transferred profiles were observed, which are characteristic of the reduction of the H_2O_2 formed during the ORR [33]. At less positive potentials than 0.5 V vs RHE, carbon materials can further reduce the H_2O_2 to H_2O molecules, increasing the number of electrons transferred [33]. Regarding the selectivity, the number of electrons transferred shows a similar profile after 25 cycles of reaction, which means that the deactivation of the catalyst does not seem to affect the reduction mechanism.

The electrocatalytic activity of the NMC samples was also studied in acid solution. The material shows an E_{ONSET} of 0.75 V vs RHE with a number of electrons transferred close to four during the whole potential range. The half-wave potential cannot be calculated because of the lack of a defined limiting current density. The lack of the diffusion-limited current plateau during these ORR experiments can be explained considering that only N species are active towards the ORR in the potential range and that their catalytic activity is significantly lower than in alkaline conditions. Thus, since the N content is small (1.4 at.%) and the catalytic activity is much lower than in alkaline conditions, not all the oxygen molecules that reach the electrode surface can be reduced.

The same cycling test was also performed in the sulphuric acid electrolyte, where similar trends were observed. The catalytic activity of NMC decreases to an E_{ONSET} of 0.65 V after 25 cycles. In the acid electrolyte, the catalytic activity impoverishment is more important than in the alkaline medium. Nevertheless, such impoverishment does not have an influence on the ORR mechanism, as confirmed by the number of electrons transferred.

Interestingly, the catalytic properties towars ORR in acidic and alkaline electrolytes show important differences in terms of activity and selectivity. The kinetics of the ORR (evaluated as E_{ONSET} or half-wave potential) shows a better performance in alkaline conditions. This is due to the high stabilization of the ORR intermediates by the protons of the acidic electrolyte, which makes difficult the completion of the following ORR steps. However, in alkaline conditions, the lack of protons surrounding the N active sites makes the ORR easier [25]. In addition, the presence of the protons surrounding the nitrogen species favours the formation of ORR intermediates that work through the 4 electrons pathway and, therefore, increase the number of electrons transferred [25].

XPS technique has been widely employed to analyze the active sites of N-doped carbon materials for ORR [34–37]. The full spectrum (Figs. S4–S7) of the XPS analysis and the O1s spectra (Figs. S8–S11) can be found in the Supporting Information. From O1s spectra, it is observed that despite the drying treatment of the sample after the ORR experiments, a small contribution of adsorbed water (at 535.6 eV [38]) is still detected in all cases. Moreover, only C=O, C–OH and adsorbed water are detected in O1s spectra, which suggests the absence of N–O species (530.2 eV [39]) in the material. On the other hand, C1s spectra before and after the electrode preparation are provided in Fig. S12. It can be observed that after the electrode preparation, Nafion is successfully introduced in the electrode since a new C1s contribution appears at 292 eV, which is characteristic of the C–F species of Nafion ® [40]. However, no differences are observed in the N1s spectra in the pristine material and after electrode preparation with Nafion (Fig. S13).

The interpretation of the electrocatalytic results is often based on the analysis of the nitrogen species in the N1s spectra before the ORR measurements. However, this might be far from the real situation since nitrogen functionalities can be modified during the reaction by the electrolyte, ORR intermediates, etc. Therefore, the most accurate XPS analysis should be done under operando conditions in order to observe which oxidation states of the functionalities predominate at the reaction potential. Unfortunately, this is not possible nowadays because of the lack of experimental tools that enable this kind of experiments with high accuracy. A second option to handle this topic is the approach followed in this work. XPS analysis has been performed before and after ORR in order to analyze the changes in the nitrogen species. The deconvolution of N1s spectra has been done according to the literature [29,41,42]; pyridines (398.5 ± 0.2 eV), N–C–O groups

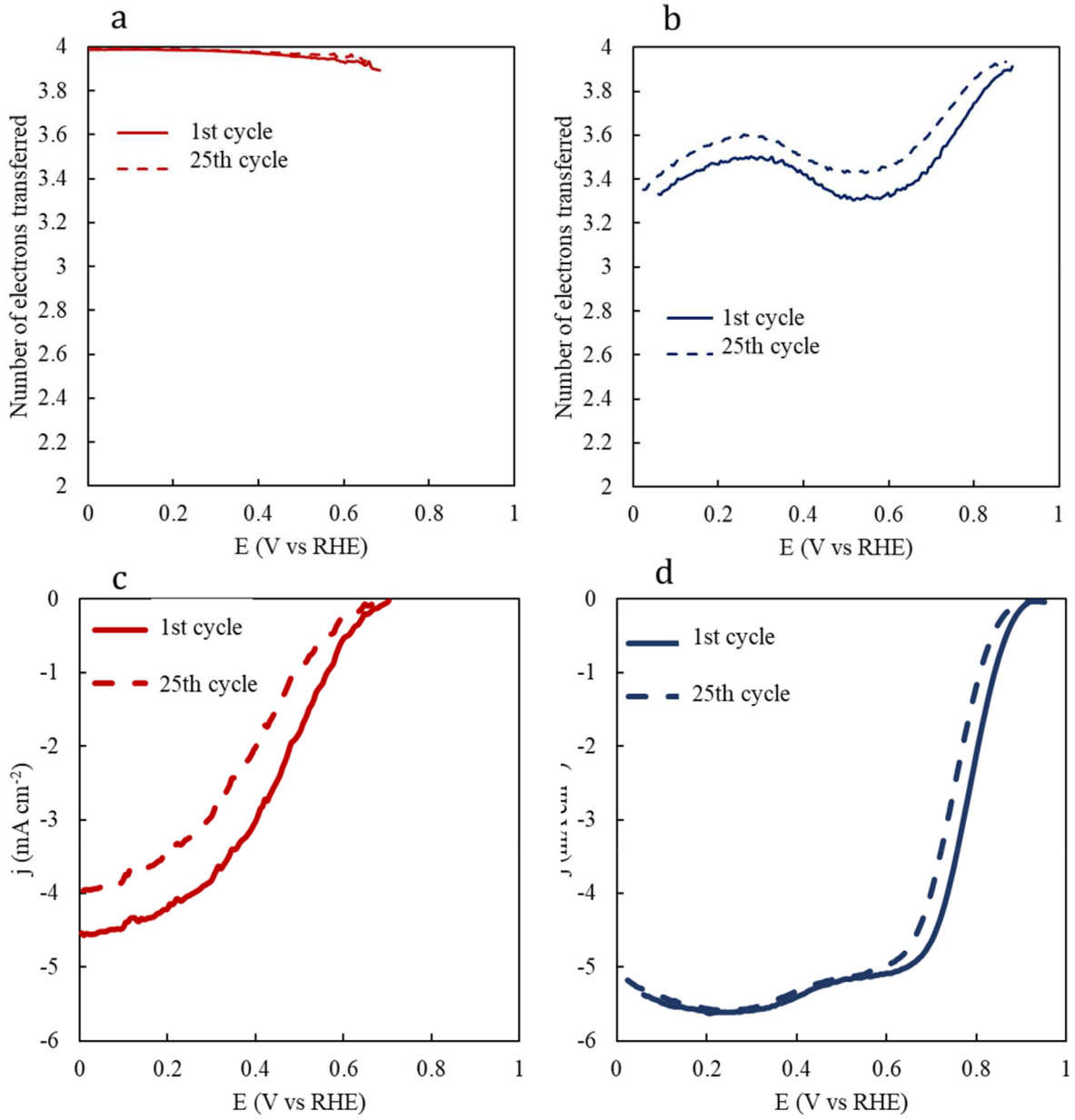

Fig. 1. a) and b) number of electrons transferred; c) and d) LSV curves for NMC. First cycle (continuous line) and after (dashed line) 25 cycles in an oxygen-saturated (red lines) 0.5 M H_2SO_4 and (blue lines) 0.1 M KOH solutions. Scan rate = 5 mV s^{-1}. Rotation speed = 1600 rpm. (A colour version of this figure can be viewed online.)

(400.2 ± 0.2 eV), graphitic nitrogen species (401.2 ± 0.2 eV) and oxidized nitrogen groups (402.9 ± 0.2 eV).

NMC sample was immersed in the working electrolyte and subjected to cyclic voltammetry measurements between 1.0 and 0.0 V vs RHE for 30 min in a N_2 and an O_2 saturated solutions. The same electrolytes were utilized: 0.1 M KOH and 0.5 M H_2SO_4 solutions for alkaline and acidic electrolytes, respectively (Fig. 2). These experiments can allow us to understand whether the changes in the oxidation states are related to the electrolyte or to the presence of O_2 during the ORR.

Fig. 2a shows that if NMC is immersed and cycled in the sulphuric acid electrolyte without oxygen in the solution (N_2-atmosphere), the sample does not significantly modify the nitrogen oxidation states, although a minimum contribution of N–C–O groups appears (below 10%). However, if the same material is cycled in the presence of an oxygen-saturated solution (O_2-atmosphere in Fig. 2a), significant changes are observed in the oxidation states of nitrogen functional groups. Cycling the pristine NMC in an oxygen-containing solution in the potential range where the ORR takes place leads to the formation of N–C–O-type species at around 400.1 eV (i.e., pyridone species), which is consistent with the literature [16,23]. This transformation from graphitic nitrogen species into N–C–O moieties can only be understood if the graphitic nitrogen functional groups are located at the edge of the carbon layers since the oxidation of the basal atoms is highly hampered in thermodynamic terms [43].

Concerning the alkaline medium (Fig. 2b), the same study has been carried out in a 0.1 M KOH solution. If the N-doped material is introduced and cycled in a N_2-saturated KOH solution, the peak related to pyridone groups appears at around 400.3 eV. Unlike in sulphuric acid, this transformation occurs in absence of dioxygen molecules. Therefore, this must be explained by the interaction

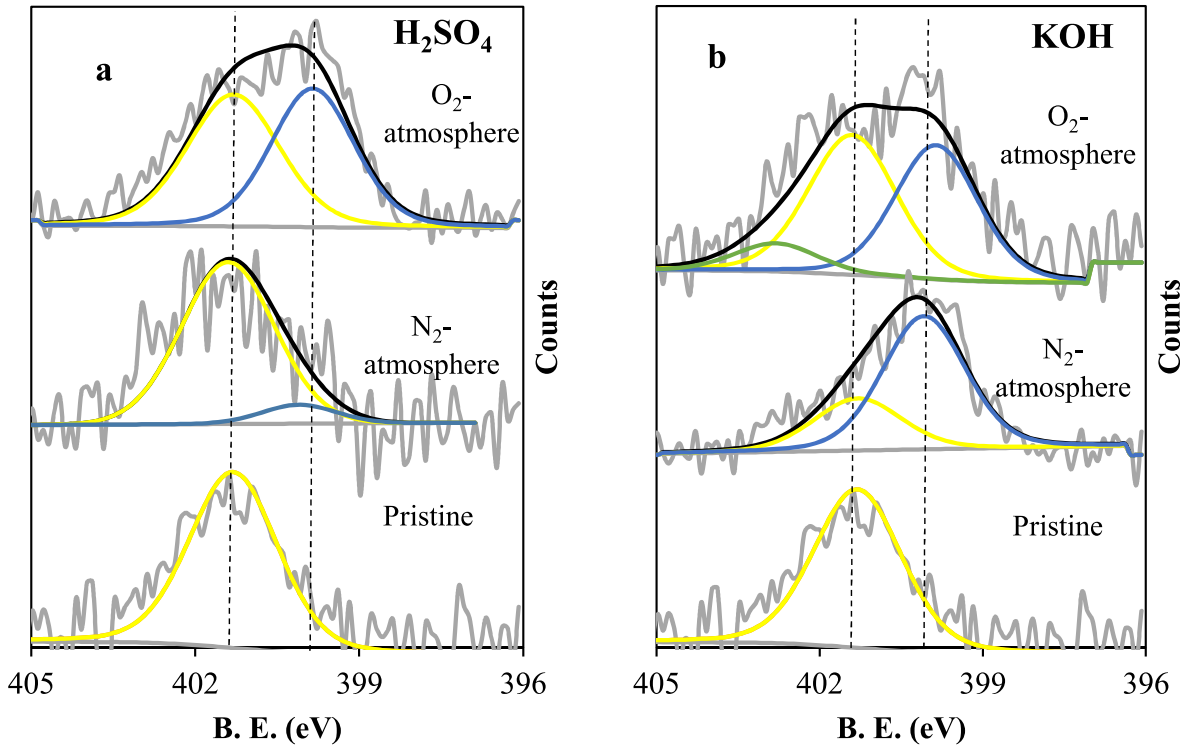

Fig. 2. N1s spectra of pristine NMC sample before and after the CV measurements in N_2-saturated atmosphere and O_2-saturated atmosphere in (a) 0.5 M H_2SO_4 and (b) 0.1 M KOH solutions. Yellow peaks represent graphitic-type contribution, while blue peaks represent N–C–O-type functionalities. (A colour version of this figure can be viewed online.)

between edge-type graphitic nitrogens and OH^- anions from the alkaline solution, thereby leading to pyridonic-type nitrogen species (i.e., N–C–O species). To confirm this assumption, the same electrode was immersed in the same KOH electrolyte at open circuit potential, resulting in the formation of N–C–O-type moieties (N1s spectrum not included for the sake of clarity). Moreover, when the material is cycled in an oxygen-containing KOH solution, there are changes in the relative contributions of the different species, but no significant new contributions appear.

XPS analysis was performed after different times in the ORR experiments for each electrolyte (Fig. 3) to evaluate how the nitrogen functionalities change with reaction time. After 5, 15 and 30 min of cycling between 1.0 and 0.0 V vs RHE, the electrodes were withdrawn from the solution, washed, dried and analyzed via XPS. On the one hand, in the H_2SO_4 solution (Fig. 3a), the observed XPS profiles show that the N–C–O species are formed over time, and the higher the reaction time, the higher the formation of such species. This might be connected to a progressive deactivation process, as observed in the decrease of the catalytic activity after 25 cycles of LSV experiments in Fig. 1. On the other hand, the behaviour of the same sample in KOH solution is quite different since the N1s spectra are more similar regardless of the reaction time measured (Fig. 3b), which indicates that the formation of N–C–O moieties starts since the immersion of the material into the alkaline electrolyte.

This is relevant since the conversion of graphitic nitrogen species into N–C–O-type groups in alkaline electrolyte seems to be mainly determined by the reaction with the electrolyte at open circuit potential conditions, making that the chemical state of the catalyst does not change significantly under reaction conditions. This may explain the less important changes in the catalytic activity in ORR experiments. However, in the acidic medium, the proportion of N–C–O-type groups significantly increases with reaction time, which leads to an essential decrease of graphitic-type nitrogen species and a more relevant deactivation in such acidic environment.

To get further insights into the possible deactivation mechanism and to elucidate the role of the applied potential, chronoamperometric analysis was performed after 30 min of working conditions at different potentials (Fig. S14). NMC was introduced into oxygen-saturated 0.5 M H_2SO_4 and 0.1 M KOH solutions at different fixed potentials and kept for 30 min. After this time, the electrode was washed with water several times, dried and analyzed via XPS. Fig. 4 shows the XPS spectra of the catalysts in both electrolytes after the chronoamperometric analysis at 0.0, 0.4, 0.6, 0.8 and 1.0 V vs RHE.

In sulphuric acid electrolyte, the XPS spectrum obtained at a fixed potential of 1.0 V vs RHE shows a significant contribution of N–C–O species (Fig. 4a). This is highly relevant since the E_{ONSET} (0.75 V vs RHE) in these conditions shows that the ORR does not occur at those positive potentials for NMC (see Fig. 1 for LSV curves). Higher overpotentials are needed for the reaction to take place. This means that the chemisorption of oxygen molecules occurs at more positive potentials than the subsequent ORR steps. Therefore, the oxygen chemisorption is not the rate limiting step in edge-type graphitic nitrogen species under these acidic conditions. This is in agreement with the prediction of a theoretical study [17] in which it was concluded that the chemisorption of dioxygen molecules is a reaction that does not need the application of overpotential in an acidic electrolyte. In order to corroborate this issue, XPS analysis of the N1s spectra was performed after open circuit potential measurements. N–C–O species are detected in an O_2-saturated sulphuric acid solution without applying an external potential (Fig. S15). This demonstrates the favourable thermodynamics of the oxygen chemisorption in sulphuric acid solution. At a less positive potential, at which the ORR commences (approximately 0.8 V vs RHE), the N1s spectrum of NMC obtained from chronoamperometric analysis significantly changes. The contribution of N–C–O groups decreases from 60% to almost 30%, which is likely related to

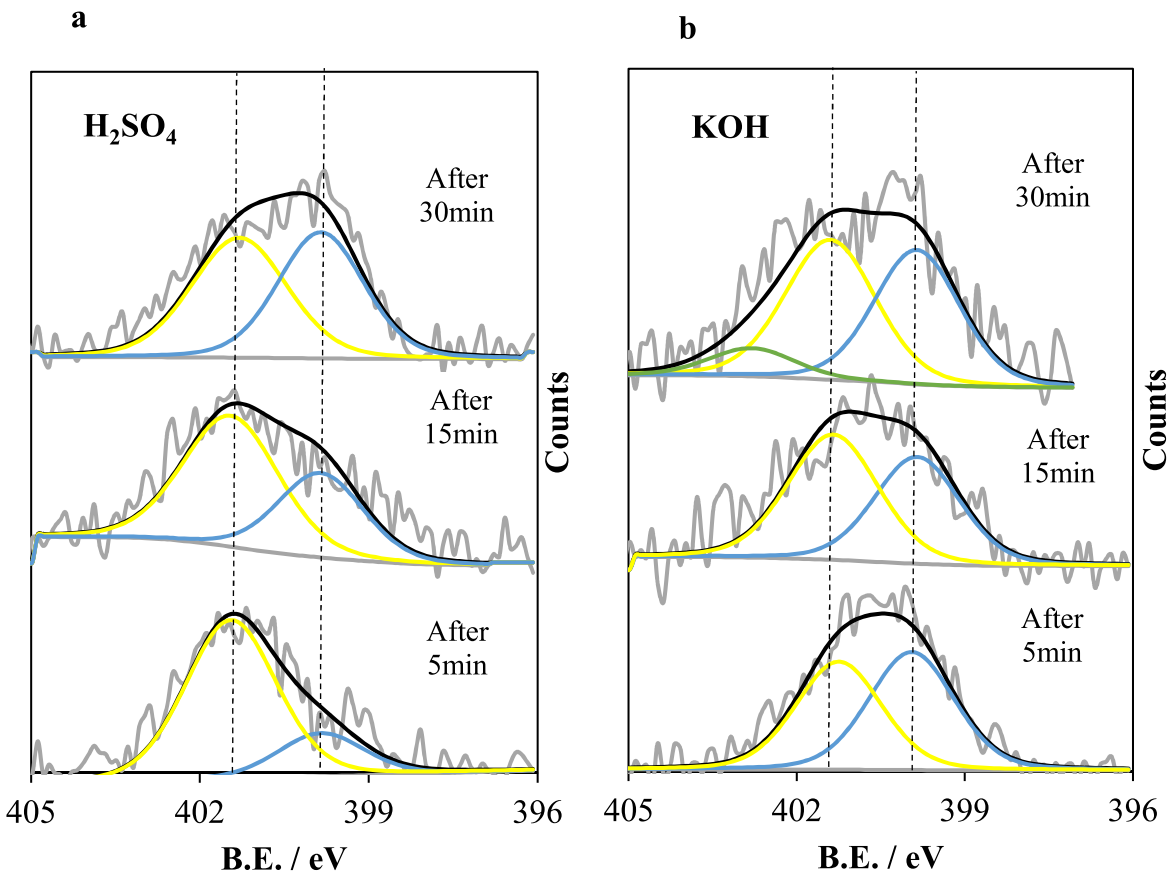

Fig. 3. N1s spectra of NMC obtained post-ORR analysis at different times: 5, 15 and 30 min in (a) 0.5 M H_2SO_4 and (b) 0.1 M KOH. Yellow peaks represent graphitic-type contribution, while blue peaks represent N–C–O-type functionalities. (A colour version of this figure can be viewed online.)

the beginning of the reduction of the dioxygen molecules that are already chemisorbed, releasing part of the active sites for further reduction processes. At potentials lower than 0.8 V, the contribution of N–C–O groups remains nearly constant in the potential range between 0.8 and 0.0 V vs RHE.

Some important points must be highlighted concerning XPS obtained from chronoamperometric results in O_2-saturated 0.1 M KOH solution (Fig. 4b). This material is highly active in the alkaline electrolyte, showing an onset potential of 0.91 V vs RHE. Interestingly, at 1.0 V vs RHE, the XPS shows that almost all nitrogen species are found as N–C–O-type groups, with a negligible contribution of graphitic-type nitrogen species. This can be explained considering the chemisorption of oxygen molecules, which can occur at more positive potentials than the reduction of dioxygen like in the sulphuric acid electrolyte, and/or the interaction of OH^- anions from the KOH electrolyte. Fig. 4b also shows that, interestingly, once the ORR commences (potentials below 0.8 V vs RHE), the contribution of N–C–O species decreases and some graphitic N-species are detected. If dioxygen molecules are already adsorbed in the active sites at more positive potentials, when decreasing the potential, the ORR can start giving rise to the release of active sites for further dioxygen reduction.

The experimental section of this work shows that the changes in edge-type graphitic nitrogen species lead to a poorer electrocatalytic performance towards the ORR in terms of E_{ONSET}, half-wave potential and current density but does not affect the number of electrons transferred. From the experimental results, the following two hypotheses can be postulated: i) the N–C–O-type groups are reaction intermediates and only graphitic-type N are those that produce high catalytic activity towards the ORR; thus, the proportion and interconversion of N–C–O/graphitic N species is what would determine the catalytic activity and ii) the N–C–O-type groups are also active towards the ORR but with a lower catalytic activity than graphitic N species. Computational modelling may help to deepen into these critical issues.

3.2. Computational modelling

Computational modelling, based on Density Functional Theory (DFT) calculations, was performed to study in detail the reaction mechanism in graphitic N containing N-doped carbon electrocatalysts.

In this sense, the most stable and preferred ORR pathways were determined for edge-type graphitic nitrogen species as they seem to be the most active nitrogen species towards the ORR. In order to take into account the effect of the electrolyte/pH, two water molecules and a continuous polarization model were included for modelling the alkaline environment, and one water molecule and one hydronium cation for modelling the acidic environment. This electrolyte environment configuration has been proved to model carbon flakes with high accuracy compared to experimental results [25]. The ORR mechanisms proposed in this section were selected according to previous DFT studies that unraveled the most favourable pathways for the ORR in each nitrogen species and

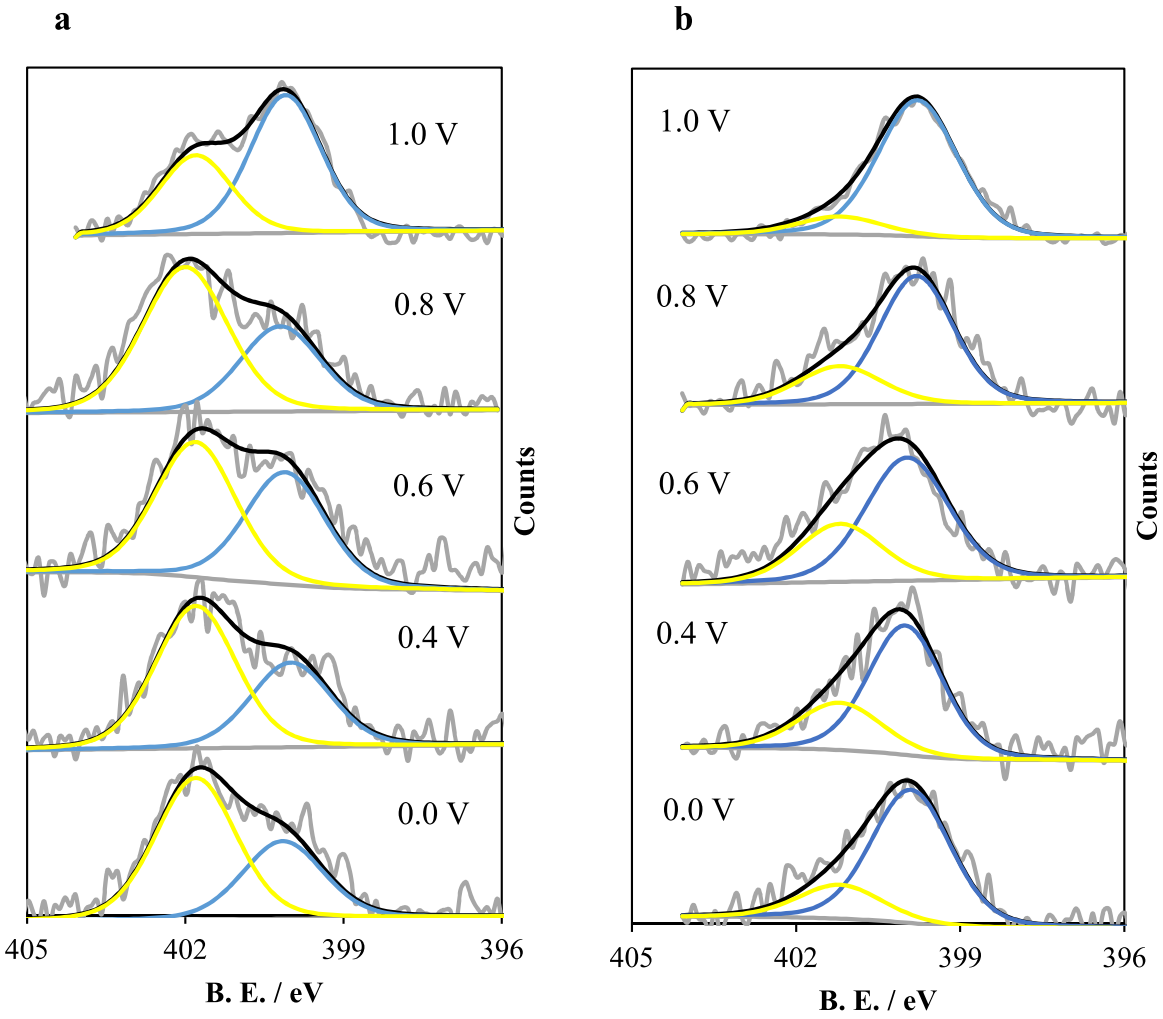

Fig. 4. N1s spectra of NMC obtained post-ORR chronoamperometric analysis at the different potential for 30 min in (a) 0.5 M H_2SO_4 solution and (b) 0.1 M KOH solution. Yellow peaks represent graphitic-type contribution, while blue peaks represent N–C–O-type functionalities. (A colour version of this figure can be viewed online.)

electrolyte [17,20,25].

3.2.1. ORR in edge-type graphitic nitrogen species

3.2.1.1. Acid medium. Fig. 5 shows the free energy diagram obtained at 1.23 V for the ORR in edge-type graphitic nitrogen for an acidic environment. The model configuration of ORR stages has been included. Moreover, a schematic representation of the possible changes of the ORR intermediates is also added in Fig. 6.

Firstly, it is important to point out that the chemisorption of oxygen molecules shows negative free energy in the acidic electrolyte, which means that the oxygen chemisorption would take place without applying an external potential. This agrees with the XPS results obtained from the chronoamperometric analysis, where at a potential of 1.0 V vs RHE, in which ORR does not occur according to LSV experimental results, the dioxygen molecules are chemisorbed in the carbon atom adjacent to the nitrogen functionality, forming N–C–O-type intermediates. This chemisorption takes place in a terminal C–O–O configuration due to the strong interactions of the chemisorbed oxygen atoms and the H^+ from the acid electrolyte, which leads to a very stable ORR intermediate [25]. Moreover, it is worth noting that, in the acidic environment, the ORR intermediate formed after the second reduction step shows a large negative free energy, which means the formation of a very stable reaction intermediate for graphitic-type nitrogen species that might make difficult the completion of the ORR [25].

To evaluate the possible deactivation mechanisms, we have considered oxidation and tautomerization pathways that may influence the ORR mechanism. The first possible deactivation mechanism of edge-type graphitic nitrogen in an acidic electrolyte that we can envision occurs after the chemisorption of the oxygen molecule (path *a1* in Fig. 6). In this case, the configuration > C(H)–O–O can be oxidized to form a triangular bridging bond in which both oxygen atoms from the dioxygen molecule are bonded to the carbon atom adjacent to the nitrogen functionality. Since such oxidation involves the transfer of an electron-proton pair, the applied potential influences the thermodynamics of this reaction [32]. This is reflected in Fig. 7, in which the ΔG of this deactivation mechanism (path *a1* in Fig. 6) and the ORR stage (stage 1 in Fig. 6) have been plotted over the applied potential. Fig. 7a shows that path *a1* seems to be a plausible deactivation mechanism for edge-type graphitic nitrogen species at positive potentials since this reaction has a larger negative free energy. As a consequence of this reaction, the active site would be oxidized, thus changing its chemical nature. However, the ORR (occurring through stage 1 in Fig. 6) is the most favourable pathway at lower potentials (interestingly at values close to the experimental values).

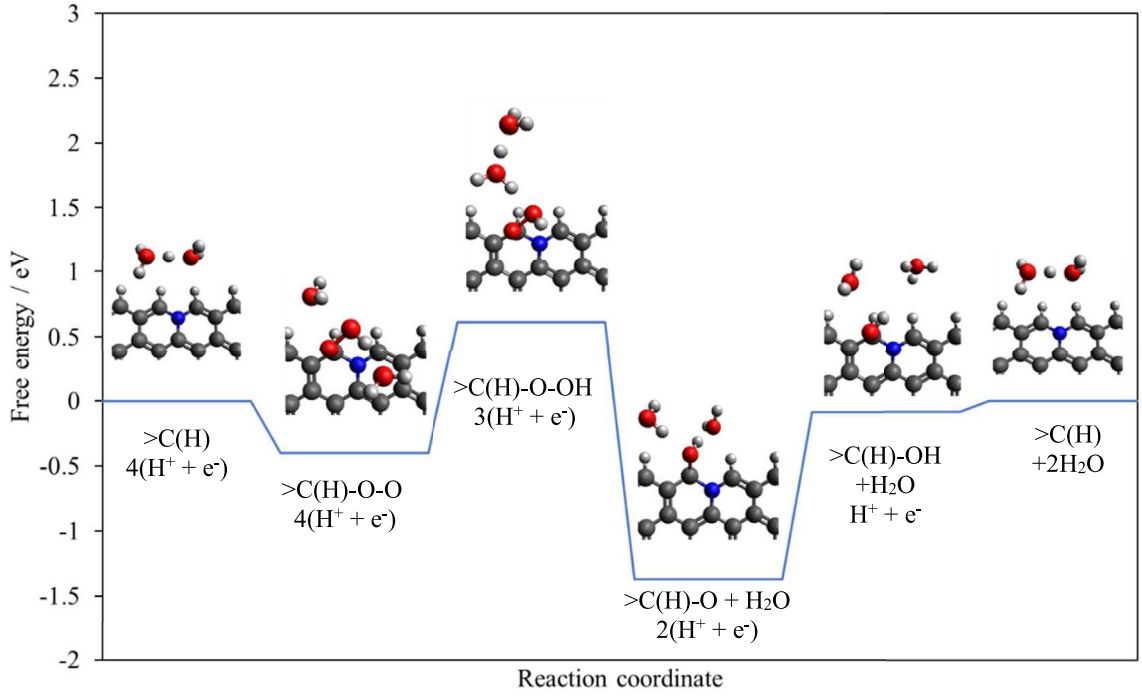

Fig. 5. Free energy diagram and model configuration of the oxygen reduction reaction stages in edge-type graphitic nitrogen functional group in acidic electrolyte at 1.23 V. (A colour version of this figure can be viewed online.)

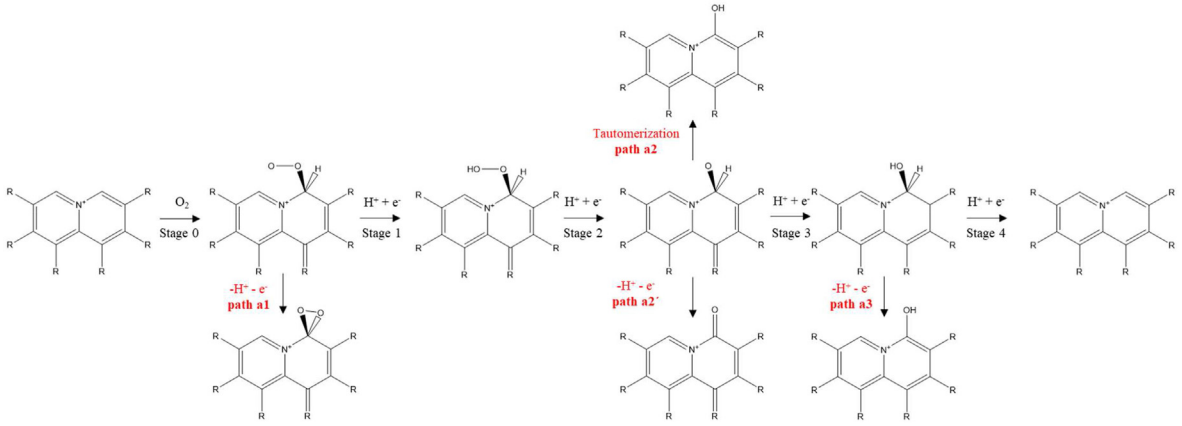

Fig. 6. Schematic representation of possible changes of the ORR intermediates in acidic electrolyte for edge-type graphitic nitrogen species. (A colour version of this figure can be viewed online.)

After the second reduction stage of the ORR, we envision two different deactivation paths; (path *a2*) which involves a tautomerization of the >C(H)–O to > C–OH and (path *a2′*) the oxidation of the >C(H)–O to > C═O, in which one electron-proton pair is involved. Fig. 7b shows the ΔG of these pathways in relation to the applied potential and the ORR (stage 3 in Fig. 6) is included for comparison purposes. Interestingly, paths *a2* and *a2′* seem to be viable routes in thermodynamic terms since the free energies of these paths are more negative than those obtained for the third oxygen reduction step. Finally, path *a3* shows the deactivation mechanism of the ORR intermediate after the third reduction stage, which can lead to the formation of >C–OH. This oxidation process also shows negative free energy for the deactivation of the edge-type nitrogen functional group; however, at lower potentials (at values close to the experimental values), the ORR stage (stage 4 in Fig. 6) is the most favourable pathway.

Interestingly, these modelling results suggest, in agreement with the experimental results and previous works, that N–C–O-type groups are intermediates formed during ORR and are thermodynamically stable [16]. However, the calculations also raise the possibility of the formation of pyridone groups (N–C–O-type groups) from the oxidation or tautomerization reactions of the ORR intermediates. Therefore, one possibility to explain the lower activity with the time of use in acidic conditions is that the oxidation or tautomerization reactions have to occur in the opposite direction for the ORR to continue (which must involve an increase in the overpotential of the ORR). The second possibility is that these pyridonic-type functional groups are also active towards the oxygen reduction reaction, although less active than the pristine graphitic N species.

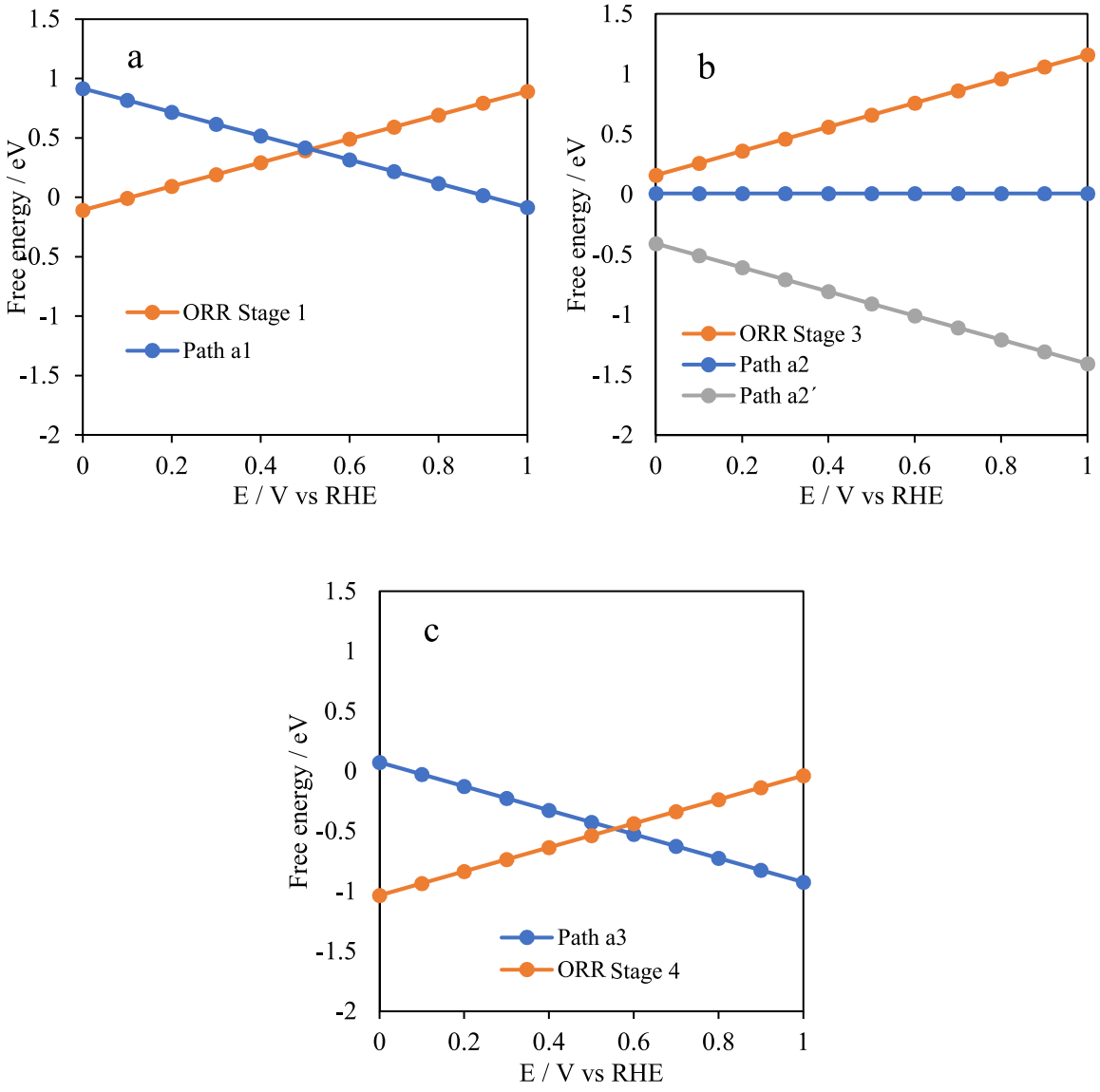

Fig. 7. Free energy vs applied potential of possible deactivation mechanisms during ORR in acidic electrolyte for edge-type graphitic nitrogen species. (A colour version of this figure can be viewed online.)

3.2.1.2. Alkaline medium. The same modelling approach has been applied for edge-type graphitic nitrogen species since N1s spectra (Fig. 2) show that both graphitic-type and N–C–O-type functionalities coexist on the surface of the material in alkaline conditions. N–C–O groups are specifically studied in the following section. In this case, two water molecules embedded in a continuous polarization model have been employed for modelling this environment. Fig. 8 shows the free energy diagram obtained at 1.23 V for the ORR in edge-type graphitic nitrogen for an alkaline environment.

It is worth noting the important differences in the free energy diagram and ORR mechanisms depending on the electrolyte employed. The acidic medium leads to very stable ORR intermediates that make the completion of the reaction much more difficult and explain the lower catalytic activity [25]. However, the absence of protons in the alkaline environment reduces these high energy requirements, leading to a more straightforward oxygen reduction reaction. This is especially remarkable in the oxygen chemisorption stage, which takes place through the formation of -C-O-O-C bridging binding mode in alkaline media. The absence of protons, which stabilize the terminal configuration in acid solution, leads to the formation of bridging bonds in an alkaline environment [25].

These free energy diagrams are consistent with those previously obtained in the literature [20], despite using different basis sets, which reinforces the observed trends in ORR for these carbon-based flakes. It should be highlighted that, unlike in the acidic electrolyte, the oxygen chemisorption step shows positive free energy. In XPS analyses, we observed that at 1.0 V vs RHE, the majority of the nitrogen species were found as N–C–O species. According to our modelling results, this cannot only be due to oxygen molecule chemisorption. Therefore, the formation of such a high concentration of N–C–O species at 1.0 V seems to be mainly related to the interaction of the OH^- anions of the electrolyte to the adjacent carbon atoms. This reaction may occur in the absence of oxygen molecules, as was demonstrated in the CV study performed in the N_2 atmosphere (Fig. 2).

Fig. 9 shows a schematic representation of the possible deactivation mechanisms that we envision for edge-type graphitic

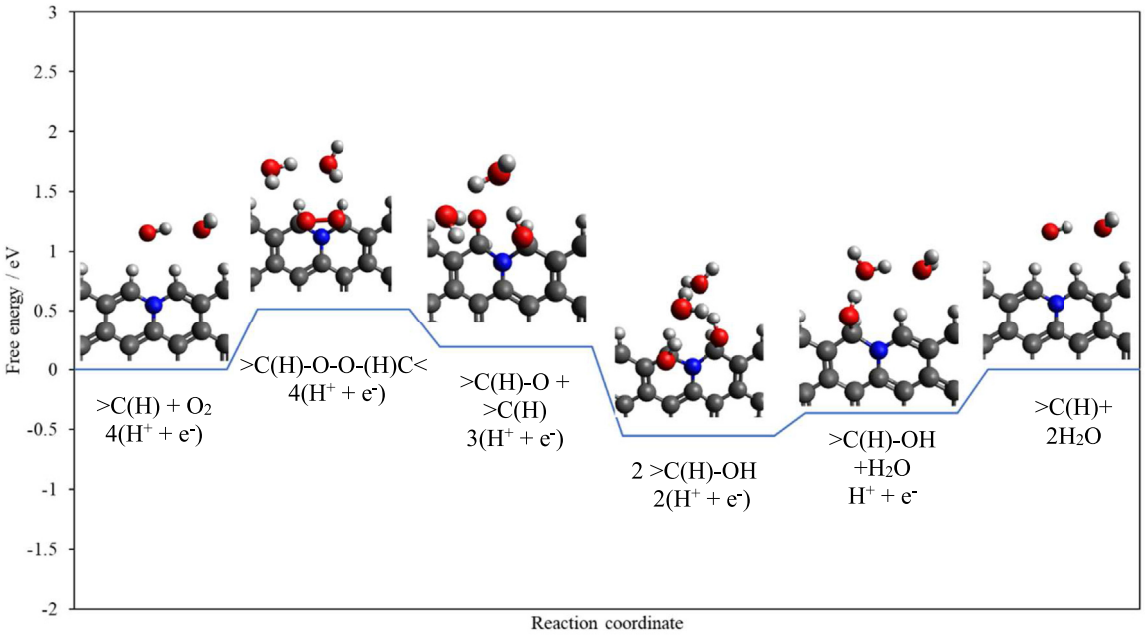

Fig. 8. Free energy diagram and model configuration of the oxygen reduction reaction stages in edge-type graphitic nitrogen functional group in alkaline electrolyte at 1.23 V. (A colour version of this figure can be viewed online.)

nitrogen species in an alkaline medium. All these possible deactivation reactions have been plotted versus the applied potential in Fig. 10.

Free energies, calculated for paths b1, b1′ and b2, have been plotted over the applied potential (Fig. 10). The modelling results show that ORR has a competitive reaction in the oxidation of edge-type graphitic nitrogen functionals groups, which is particularly noteworthy at positive potentials, and that may hamper the completion of the oxygen reduction, or modify the reaction mechanism. This process leads to changes in the oxidation states of the pristine nitrogen species. In addition, tautomerization reaction (path b1′) can also compete against the ORR. Interestingly, all these deactivation/oxidation mechanisms are thermodynamically viable.

The comparison of the free energy diagrams in acidic and alkaline environments (Figs. 5 and 8) sheds light on the possible differences in deactivation depending on the electrolyte. In the acidic environment, the ORR intermediates are much more stable, with much larger negative energies for the reaction intermediates, which makes the kinetics of the reaction slower than in alkaline conditions. In addition, since the oxidation and tautomerization reactions have proven to be possible in both environments, the high stability of the ORR intermediates in the acidic electrolyte gives a larger amount of time for the intermediate oxidation or tautomerization and, consequently, for its deactivation or for evolving through a more inefficient reaction mechanism. This agrees with experimental results since the deactivation observed in ORR experiments is higher in such a protonic environment (LSV curves in Fig. 1).

However, in the alkaline environment, it was observed that the formation of N–C–O species already occurs by the reaction with

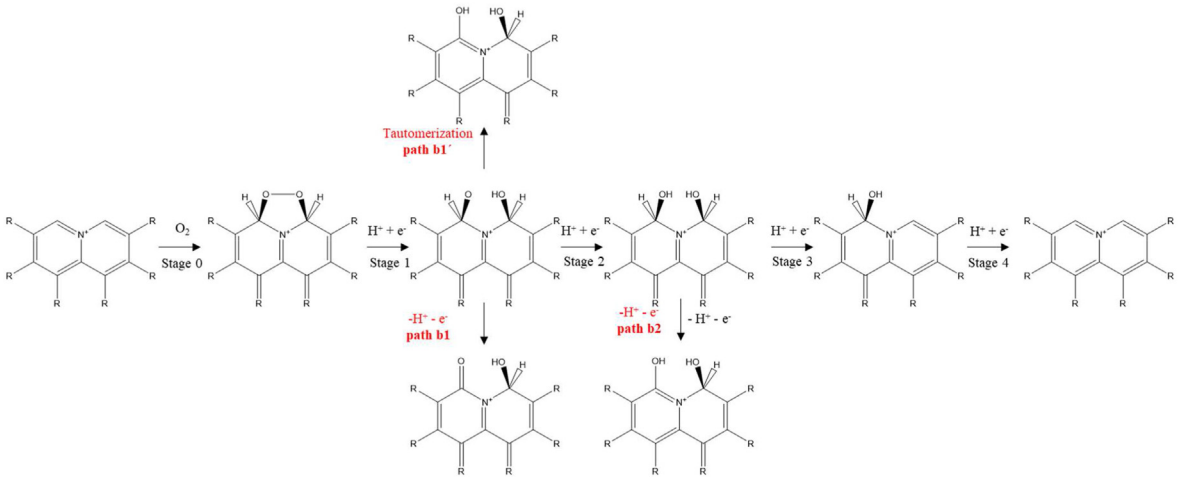

Fig. 9. Schematic representation of possible changes of the ORR intermediates in alkaline electrolyte for edge-type quaternary nitrogen species. (A colour version of this figure can be viewed online.)

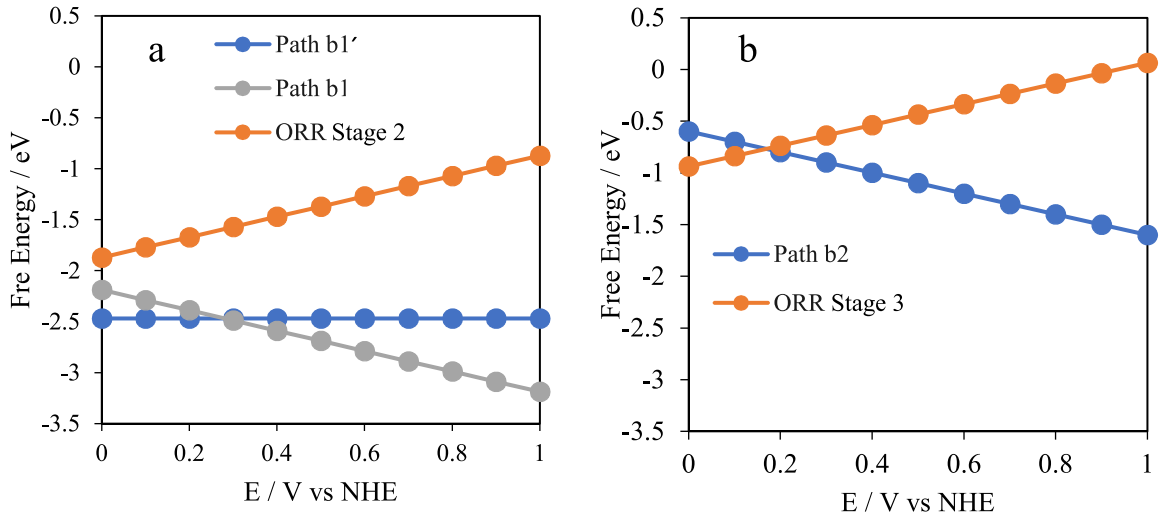

Fig. 10. Free energy vs applied potential of possible deactivation mechanisms during ORR in alkaline electrolyte for edge-type graphitic nitrogen species. (A colour version of this figure can be viewed online.)

the electrolyte in the absence of oxygen molecules and that the proportion of graphitic nitrogen and N–C–O-type groups remains nearly constant from the beginning until the end of the ORR experiments (see Fig. 3 that shows XPS results after cycling tests). Consequently, no important differences are observed in the catalytic activity. These results suggest that the N–C–O and graphitic N species coexist and act as active sites in the ORR in the alkaline medium. For this reason, in the following section, we consider the ORR in N–C–O species as active sites in both electrolytes.

These results in acidic and alkaline solutions show interesting discrepancies with a previous work in which a non-H-terminated carbon cluster was used [24]. This previous work obtained positive free energy for the deactivation mechanisms. In contrast, our work shows thermodynamically viable mechanisms for the deactivation of the active sites in the ORR, highlighting the necessity of including H-terminated carbon clusters in the calculations for carbon-based electrocatalysts.

3.2.2. *ORR in N–C–O-type species*

Fig. 11a and b shows the optimized geometries for N–C–O-type species in the acidic and alkaline electrolyte, respectively. Fig. 11c and d shows the free energy diagrams obtained at different potentials for the ORR in N–C–O-type groups for the acidic and alkaline electrolyte, respectively. It is observed that the free energies of the ORR processes at 1.23 V (black lines) are higher in comparison with those of edge-type graphitic nitrogen species in both alkaline and acidic medium (see Figs. 5 and 8 for comparison purposes). Nevertheless, when the potential is applied, it is observed that the free energies of ORR in N–C–O groups in the alkaline environment (Fig. 11d) become mostly negative, which explains their competitive activity towards the ORR, which may be even close to that of graphitic-N type functional groups.

However, the profile in the acidic environment (Fig. 11c) still shows large positive free energies even when the same potential is applied. This is particularly noteworthy in the oxygen molecule chemisorption stage, which occurs in the non-oxidized carbon atom adjacent to the nitrogen heteroatom (red arrows in Fig. 11a). The chemisorption of the dioxygen molecules in N–C–O-type groups shows a very positive free energy in an acidic environment, which means that the chemisorption is very difficult. This is very different from what is observed in the pristine edge-type graphitic nitrogen groups (see Fig. 5), in which the chemisorpion may occur having a negative free energy. On the other hand, Fig. 11d shows that the free energies for the ORR steps for the N–C–O-type groups show a more competitive profile towards the ORR in the alkaline environment, since the energy of the oxygen molecule chemisorption stage is almost zero and after the application of an overpotential the free energies of the rest of the ORR steps mainly became negative.

Therefore, in the acidic environment, the deactivation of graphitic-type nitrogen species seems to be mainly due to the formation of N–C–O species through oxidation and tautomerization reactions of the ORR intermediates. These species show a poor catalytic activity towards the ORR in a protonic environment, being especially difficult the oxygen chemisorption. Consequently, the catalytic activity of the N-doped carbon materials in an acidic solution is governed by the interconversion of graphitic-type groups into N–C–O-type nitrogen species. On the other hand, in the alkaline environment, there exists a coexistence of both N–C–O and graphitic-type groups due to the interaction of the pristine graphitic nitrogen species with the OH^- anions of the electrolyte. The relative amount of these species remains nearly constant with the time of reaction. Moreover, N–C–O-type nitrogen groups seem to be almost as active as graphitic-type nitrogen functional in such an environment, which can explain the lower deactivation observed for the graphitic N-doped carbon materials in the alkaline electrolyte. This agrees with the literature since N–C–O species have also been proposed as active sites towards the ORR in an alkaline environment [9,44].

4. Conclusions

This work has tried to shed light in the identification of the active sites of N-doped carbon materials in alkaline and acidic electrolytes during ORR through a combination of computational modelling and experimental results. We have prepared a N-doped carbon material with essentially one nitrogen species: graphitic nitrogen functional groups. This has been used as an ideal model to unravel the state of the nitrogen species at ORR conditions. The extended characterization via XPS and the computational

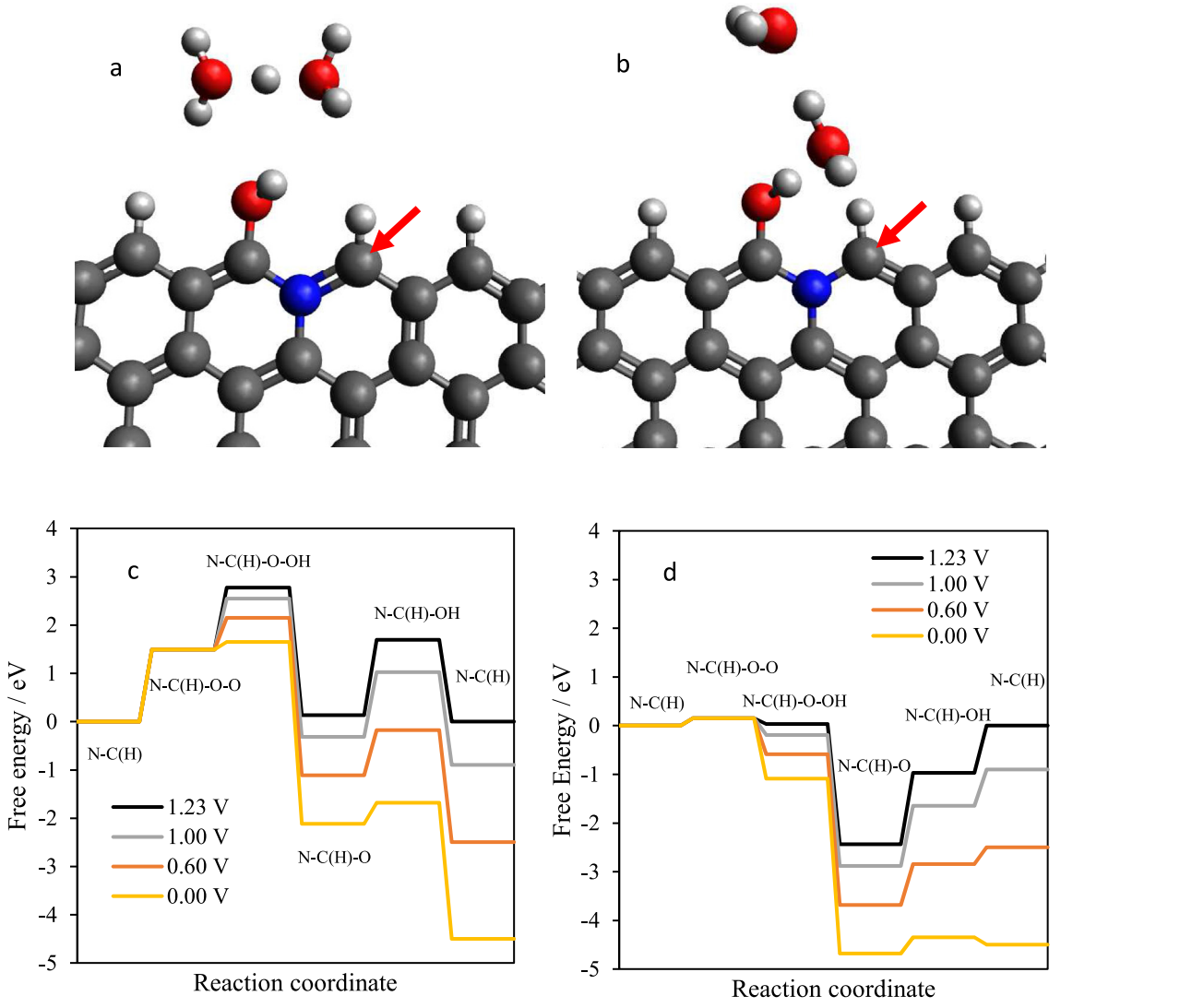

Fig. 11. Optimized geometry of the N–C–O groups in (a) acidic and (b) alkaline electrolyte. Free energy diagram and model configuration of the oxygen reduction reaction stages in N–C–O groups in zigzag position for (c) acidic and (d) alkaline electrolyte. (A colour version of this figure can be viewed online.)

modelling show that graphitic-type nitrogen species experience oxidation and tautomerization reactions that result in the formation of N–C–O-type groups during the ORR in both acidic and alkaline environments. According to the results, this has different consequences depending on the electrolyte. In an acidic environment, the ORR kinetics is slower due to the high stability of the ORR intermediates. These reaction intermediates can be converted into N–C–O-type groups, which have a poor activity towards ORR in a protonic environment, thus explaining the significant deactivation in an acidic electrolyte.

On the other hand, in an alkaline electrolyte, the N–C–O-type groups can be easily formed due to the interaction of graphitic-type N species and the OH^- anions from the electrolyte. In this case, the catalytic activity is due to the contribution of both graphitic nitrogen groups and N–C–O species. The catalytic activity of N–C–O groups in an alkaline electrolyte is similar to that of graphitic N groups.

Author contribution

J.Q.B, E.M and D.C.A contributed equally to the design and implementation of the research, to the analysis of the results and to the writing of the manuscript

Declaration of competing interest

The authors declare that they have no known competing financial interests or personal relationships that could have appeared to influence the work reported in this paper.

Acknowledgements

The authors would like to thank MICINN and FEDER (projects PID2019-105923RB-100 and RTI2018-095291-B-I00) for the financial support.

Appendix A. Supplementary data

Supplementary data to this article can be found online at https://doi.org/10.1016/j.carbon.2021.12.086.

References

[1] X.X. Wang, M.T. Swihart, G. Wu, Achievements, challenges and perspectives on cathode catalysts in proton exchange membrane fuel cells for transportation, Nat. Catal. 2 (2019) 578–589.

[2] E.H. Majlan, D. Rohendi, W.R.W. Daud, T. Husaini, M.A. Haque, Electrode for proton exchange membrane fuel cells: a review, Renew. Sustain. Energy Rev. 89 (2018) 117–134.

[3] A. Kulkarni, S. Siahrostami, A. Patel, J.K. Nørskov, Understanding catalytic activity trends in the oxygen reduction reaction, Chem. Rev. 118 (2018) 2302–2312.

[4] Z.F. Pan, L. An, T.S. Zhao, Z.K. Tang, Advances and challenges in alkaline anion exchange membrane fuel cells, Prog. Energy Combust. Sci. 66 (2018) 141–175.

[5] A.A. Gewirth, J.A. Varnell, A.M. Diascro, Nonprecious metal catalysts for oxygen reduction in heterogeneous aqueous systems, Chem. Rev. 118 (2018) 2313–2339.

[6] A. Morozan, B. Jousselme, S. Palacin, Low-platinum and platinum-free catalysts for the oxygen reduction reaction at fuel cell cathodes, Energy Environ. Sci. 4 (2011) 1238–1254.

[7] O. Lori, L. Elbaz, Recent advances in synthesis and utilization of ultra-low loading of precious metal-based catalysts for fuel cells, ChemCatChem 12 (2020) 3434–3446.

[8] A. Kongkanand, M.F. Mathias, The priority and challenge of high-power performance of low-platinum proton-exchange membrane fuel cells, J. Phys. Chem. Lett. 7 (2016) 1127–1137.

[9] J. Quílez-Bermejo, C. González-Gaitán, E. Morallón, D. Cazorla-Amorós, Effect of carbonization conditions of polyaniline on its catalytic activity towards ORR. Some insights about the nature of the active sites, Carbon 119 (2017) 62–71.

[10] J. Quílez-Bermejo, E. Morallón, D. Cazorla-Amorós, Oxygen-reduction catalysis of N-doped carbons prepared: via heat treatment of polyaniline at over 1100 °c, Chem. Commun. 54 (2018) 4441–4444.

[11] Q. Wei, X. Tong, G. Zhang, J. Qiao, Q. Gong, S. Sun, Nitrogen-doped carbon nanotube and graphene materials for oxygen reduction reactions, Catalysts 5 (2015) 1574–1602.

[12] K. Gao, B. Wang, L. Tao, B.V. Cunning, Z. Zhang, S. Wang, R.S. Ruoff, L. Qu, Efficient metal-free electrocatalysts from N-doped carbon nanomaterials: mono-doping and Co-doping, Adv. Mater. 31 (2019) 1805121.

[13] S. Maldonado, K.J. Stevenson, Influence of nitrogen doping on oxygen reduction electrocatalysis at carbon nanofiber electrodes, J. Phys. Chem. B 109 (2005) 4707–4716.

[14] K. Gong, F. Du, Z. Xia, M. Durstock, L. Dai, Nitrogen-doped carbon nanotube arrays with high electrocatalytic activity for oxygen reduction, Science 323 (2009) 760–764.

[15] J.D. Wiggins-Camacho, K.J. Stevenson, Mechanistic discussion of the oxygen reduction reaction at nitrogen-doped carbon nanotubes, J. Phys. Chem. B 115 (2011) 20002–20010.

[16] D. Guo, R. Shibuya, T. Kondo, J. Nakamura, Active sites in nitrogen-doped carbon materials for oxygen reduction reaction, Science 351 (2016) 361–365.

[17] T. Ikeda, M. Boero, S.F. Huang, K. Terakura, M. Oshima, J. Ozaki, Carbon alloy catalysts: active sites for oxygen reduction reaction, J. Phys. Chem. C 112 (2008) 14706–14709.

[18] S.F. Huang, K. Terakura, T. Ozaki, T. Ikeda, M. Boero, M. Oshima, J.I. Ozaki, S. Miyata, First-principles calculation of the electronic properties of graphene clusters doped with nitrogen and boron: analysis of catalytic activity for the oxygen reduction reaction, Phys. Rev. B Condens. Matter 80 (2009) 235410.

[19] H. Kim, K. Lee, S.I. Woo, Y. Jung, On the mechanism of enhanced oxygen reduction reaction in nitrogen-doped graphene nanoribbons, Phys. Chem. Chem. Phys. 13 (2011) 17505–17510.

[20] J. Quílez-Bermejo, M. Melle-Franco, E. San-Fabián, E. Morallón, D. Cazorla-Amorós, Towards understanding of the active sites for ORR in N-doped carbon materials through a fine-tuning of nitrogen functionalities: an experimental and computational approach, J. Mater. Chem. A. 7 (2019) 24239–24250.

[21] J. Quílez-Bermejo, E. Morallón, D. Cazorla-Amorós, Metal-free heteroatom-doped carbon-based catalysts for ORR: a critical assessment about the role of heteroatoms, Carbon 165 (2020) 434–454.

[22] H. Singh, S. Zhuang, B. Ingis, B.B. Nunna, E.S. Lee, Carbon-based catalysts for oxygen reduction reaction: a review on degradation mechanisms, Carbon 151 (2019) 160–174, 75.

[23] T. Xing, Y. Zheng, L.H. Li, B.C.C. Cowie, D. Gunzelmann, S.Z. Qiao, S. Huang, Y. Chen, Observation of active sites for oxygen reduction reaction on nitrogen-doped multilayer graphene, ACS Nano 8 (2014) 6856–6862.

[24] N. Yang, L. Peng, L. Li, J. Li, Z. Wei, Theoretical research on the oxidation mechanism of doped carbon based catalysts for oxygen reduction reaction, Phys. Chem. Chem. Phys. 21 (2019) 26102–26110.

[25] J. Quílez-Bermejo, K. Strutynski, M. Melle-Franco, E. Morallón, D. Cazorla-Amorós, On the origin of the effect of pH in ORR for non-doped and edge-type quaternary N-doped metal-free carbon-based catalysts, ACS Appl. Mater. Interfaces 12 (2020) 54815–54823.

[26] J. Quílez-Bermejo, A. Ghisolfi, D. Grau-Marín, E. San-Fabián, E. Morallón, D. Cazorla-Amorós, Post-synthetic efficient functionalization of polyaniline with phosphorus-containing groups. Effect of phosphorus on electrochemical properties, Eur. Polym. J. 119 (2019) 272–280.

[27] T. Sharifi, G. Hu, X. Jia, T. Wågberg, formation of active sites for oxygen reduction reactions by transformation of nitrogen functionalities in nitrogen-doped carbon nanotubes, ACS Nano 6 (2012) 8904–8912.

[28] J.R. Pels, F. Kapteijn, J.A. Moulijn, Q. Zhu, K.M. Thomas, Evolution of nitrogen functionalities in carbonaceous materials during pyrolysis, Carbon 33 (1995) 1641–1653.

[29] E. Raymundo-Piñero, D. Cazorla-Amorós, A. Linares-Solano, J. Find, U. Wild, R. Schlögl, Structural characterization of N-containing activated carbonfibers prepared from a low softening point petroleum pitch anda melamine resin, Carbon 40 (2002) 597–608.

[30] M.J. Frisch, G.W. Trucks, H.B. Schlegel, G.E. Scuseria, M.A. Robb, , et al.J.R. Cheeseman, Gaussian 09, Revision D. 01, Gaussian, Inc., Wallingford CT, 2016.

[31] M. Reda, H.A. Hansen, T. Vegge, DFT study of stabilization effects on N-doped graphene for ORR catalysis, Catal. Today 312 (2018) 118–125.

[32] J.K. Nørskov, J. Rossmeisl, A. Logadottir, L. Lindqvist, J.R. Kitchin, T. Bligaard, H. Jónsson, Origin of the overpotential for oxygen reduction at a fuel-cell cathode, J. Phys. Chem. B 108 (2004) 17886–17892.

[33] A. Gabe, R. Ruiz-Rosas, C. González-Gaitán, E. Morallón, D. Cazorla-Amorós, Modeling of oxygen reduction reaction in porous carbon materials in alkaline medium. Effect of microporosity, J. Power Sources 412 (2019) 451–464.

[34] K.H. Wu, D.W. Wang, D.S. Su, I.R. Gentle, A discussion on the activity origin in metal-free nitrogen-doped carbons for oxygen reduction reaction and their mechanisms, ChemSusChem 8 (2015) 2772–2788.

[35] S. Wang, Z. Teng, C. Wang, G. Wang, Stable and efficient nitrogen-containing carbon-based electrocatalysts for reactions in energy-conversion systems, ChemSusChem 11 (2018) 2267–2295.

[36] S.K. Singh, K. Takeyasu, J. Nakamura, Active sites and mechanism of oxygen reduction reaction electrocatalysis on nitrogen-doped carbon materials, Adv. Mater. 31 (2019) 1804297.

[37] J. Quílez-Bermejo, E. Morallón, D. Cazorla-Amorós, Polyaniline-derived N-doped ordered mesoporous carbon thin films: efficient catalysts towards oxygen reduction reaction, Polymers 12 (2020) 2382.

[38] S.D. Gardner, C.S.K. Singamsetty, G.L. Booth, G.R. He, Surface characterization of carbon fibers using angle-resolved XPS and ISS, Carbon 33 (1995) 587–595.

[39] R. Chulliyote, H. Hareendrakrishnakumar, M. Raja, J.M. Gladis, A.M. Stephan, Sulfur-immobilized nitrogen and oxygen Co-doped hierarchically porous biomass carbon for lithium-sulfur batteries: influence of sulfur content and distribution on its performance, Chem. Sel. 2 (2017) 10484–10495.

[40] G. Nansé, E. Papirer, P. Fioux, F. Moguet, A. Tressaud, Fluorination of carbon blacks: an X-ray photoelectron spectroscopy study : I. A literature review of XPS studies of fluorinated carbons. XPS investigation of some reference compounds, Carbon 35 (1997) 175–194.

[41] D. Salinas-Torres, S. Shiraishi, E. Morallón, D. Cazorla-Amorós, Improvement of carbon materials performance by nitrogen functional groups in electrochemical capacitors in organic electrolyte at severe conditions, Carbon 82 (2015) 205–213.

[42] S. Biniak, G. Szymański, J. Siedlewski, A. Światkowski, The characterization of activated carbons with oxygen and nitrogen surface groups, Carbon 35 (1997) 1799–1810.

[43] L.R. Radovic, C.V. Mora-Vilches, A.J.A. Salgado-Casanova, A. Buljan, Graphene functionalization: mechanism of carboxyl group formation, Carbon 130 (2018) 340–349.

[44] R. Silva, D. Voiry, M. Chhowalla, T. Asefa, Efficient metal-free electrocatalysts for oxygen reduction: polyaniline-derived N- and O-doped mesoporous carbons, J. Am. Chem. Soc. 135 (2013) 7823–7826.